

## CPW Fed Wideband Bowtie Slot Antenna on PET Substrate

Manjurul A. Riheen\*, Tuan T. Nguyen, Tonmoy K. Saha,  
Tutku Karacolak, and Praveen K. Sekhar

**Abstract**—In this article, a new wideband bowtie shaped slot antenna is realized on a flexible polyethylene terephthalate (PET). The slotted bowtie design is implemented with an asymmetric bowtie flare angle and a larger feeding neck with a metal strip inside the bowtie slot to achieve a wider bandwidth and a higher gain. The designed free space antenna is fabricated using inkjet printing and tested. The fabricated antenna operates over 2.1–4.35 GHz frequency range (69.77% fractional bandwidth) which covers WLAN, WiMax, and most of the 3G and 4G frequency bands. Further, the antenna exhibits an omnidirectional radiation pattern with a peak gain of 6.3 dBi at 4.35 GHz. The bending test of the fabricated device reveals adequate flexibility without significant antenna performance degradation. Moreover, the antenna tunability for any mounting structure application is also investigated by simulating another version of the parent antenna (free space antenna) for drywall mounting applications. The tuned antenna covers a similar frequency band as a free space antenna maintaining the desired radiation performances. The compact size, higher bandwidth, omnidirectional pattern with a higher peak gain and flexible properties make the antenna design suitable for mounting structure for Internet of Things (IoT) applications.

### 1. INTRODUCTION

Internet of Things (IoT) devices are nonstandard computing devices that connect wirelessly to a network and have the ability to transmit data. Connected devices are part of a framework in which every device talks to other related devices in an environment that facilitates automated decision making [1–4]. Such an integrated platform is seeing a surge in the number of devices connected from sensors to electronic products, to name a few. To keep up with the interoperability of the dense system variants, a large number of communication devices are needed. Large deployment of IoT systems requires robust wireless platforms that are cost-effective.

As budgets and devices shrink to accommodate integrated devices, flexible and conformable substrates which offer device implementation with smaller footprint are on the rise. With the advent of flexible electronics, flexible antennas have been intensely investigated. Apart from IoT applications, flexible antennas find mandatory use in point-of-care and on-body sensing applications. In this context, the use of inexpensive and flexible substrates, along with innovative manufacturing techniques, have been leveraged to reduce the cost of the antennas [5]. Inkjet printing is a single step, economic (cost per square meter) and non-contact process of fabricating complex patterns. Several antennas have been reported in recent years that employed inkjet printing on flexible substrates [5–9].

Mansour et al. [6] and Anagnostou et al. [7] reported coplanar waveguide (cpw) fed conformal antennas inkjet printed on paper substrate. Abutarboush and Shamim [5] investigated a U Slot multilayer paper-based antenna that operates in tri-band (1.57, 3.2, and 5 GHz) at the expense of

---

*Received 14 March 2020, Accepted 16 April 2020, Scheduled 24 April 2020*

\* Corresponding author: Manjurul Ahsan Riheen (m.riheen@wsu.edu).

The authors are with the School of Engineering and Computer Science, Washington State University Vancouver, Vancouver, Washington, USA.

gain. PET-based inkjet printed flexible antennas at 2.4 GHz band were proposed by Paracha et al. [2], Hassan et al. [8], and Guo et al. [9]. Moreover, inkjet printed antennas on textile substrates can also be found in the literature [27–29]. However, most of these antennas have not achieved enough bandwidth at multiple frequency bands for practical applications. IoT devices typically require a single antenna that can operate over different communication bands like LTE, WLAN (IEEE 802.11 a/b/g/n), WiMAX (IEEE 802.16), ZigBee (IEEE 802.15.4) [30]. Integrating multiple antennas each operating at different frequency bands might be an alternative solution. Such a solution will have a performance-footprint trade-off. Further, sensors and actuators in an IoT framework might require a short response time [31]. Wideband antennas facilitate a rapid wireless system.

Because of the wideband characteristics and better impedance matching, printed bowtie slot antennas have received significant attention for wireless communications compared to the traditional microstrip antennas. Several techniques were investigated to increase the bandwidth of the bowtie slot antennas. Chen et al. [16] proposed an antenna with two metal sectors inside the bowtie slots, which generates a broader impedance bandwidth of up to 80%. Adding a meander shaped slot to the bowtie slot antennas facilitated ultra-wideband operation at the expense of increased antenna size [32]. Sallam

**Table 1.** Literature summary of performance of the bowtie antennas designed on both rigid and flexible substrates at different frequency band.

Reference	$\epsilon_r$	Flexibility	Size (mm)	Operating range (GHz)	FBW %	Peak gain (dB)
Huang et al. [10]	4.4	X	50 × 50	3.10–12	117.8	7.1
Bhaskar et al. [11]	4.3, 2.2	X	91 × 54	1.70–4.50; 2.70–5.70	90.3; 71.4	6, 7
Mazaheri et al. [12]	2.33	X	65 × 38.6	6.45–16.63	84	8
Pierce et al. [13]	2.2	X	76 × 44	4.6–8.09	54	7.71
Tsai et al. [14]	4.4	X	60 × 45	2.17–2.5; 4.98–6.31	14.13; 23.38	2.55, 3.65
Xu et al. [15]	2.2	X	53 × 25.25	2.76–8.1	100.4	5.53
Chen et al. [16]	4.9	X	30 × 26	9.5–22.4	80	-
Yoon et al. [17]	4.4	X	35 × 35	2.32–3.72; 4.93–6.23	46.56; 23.4	1.36
Dayo et al. [18]	2.17	X	30 × 60	2.7–3.5; 7.0–8.0; 9.6–10.6	25.8; 13.3; 9.9	6.9
Yamamoto et al. [19]	2.17	X	60 × 30	7.0–10.0	35.3	7.5
Sagnard et al. [20]	4.4	X	503 × 220	0.4–1.5	115.7	6
Sallam et al. [21]	3.38	✓	80 × 60	2.2–4.0	57.7	6.2
Liu et al. [22]	2.2	✓	55 × 25	3.4–3.6; 7.4–14.4	6; 64.22	NA
Sahoo et al. [23]	2.2	✓	120 × 120	0.75–1.78	81.4	4.78
Durgun et al. [24]	7, 3	✓	39 × 24.57	6.8 to 8.3	8.92	1.7
Farooqui et al. [25]	1.9	✓	88 × 44	1.48–1.7; 2.54–3	13.8; 16.6	0.8
Chowdhary et al. [26]	3.38	✓	80 × 60	3.0–4.87	59.5	7.82

et al. [21] reported a bowtie flexible antenna with a 57.7% impedance bandwidth for WLAN and WiMax application. A fishtail shaped dual-band bowtie antenna was reported by Liu et al. for WiMax and X band application [22]. In another study, the bowtie slot antenna with two symmetrical circular vias in the slots was introduced to increase bandwidth (84%) [12]. Qu and Ruan [33] reported the effect of round corners to flatten the input impedance and improve the return loss. Besides, tuning stubs were added in the bowtie slot structure for dual [14] or triple [17] band operation. Table 1 presents a concise literature review of bowtie antennas designed on rigid and flexible substrates in the last ten years.

This work aims to explore a new wideband bowtie slot antenna designed on a thin and flexible PET substrate operating from 2.1 GHz to 4.35 GHz. Though a plethora of conformal antennas have been reported on textile [27, 28] and paper [7, 34] substrate, the reason behind the choice of PET substrate is its low tangent loss and good conformal properties [9, 35–37]. Unlike textile materials, PET substrate is minimally affected by fluid absorptions, wrinkles, and pattern discontinuities. To the best of our knowledge, this is the first time a bowtie slot antenna is implemented on a flexible PET substrate. In this work, two versions of the antenna are simulated: the first case (parent antenna) corresponds to a bowtie slot antenna in free space, and the second one takes into consideration the presence of a drywall (plasterboard/wallboard) as a mounting structure of the antenna (to demonstrate the easy tunability of the proposed design to mount on any supporting surface). The free space antenna was fabricated and measured to validate the design. The proposed design is characterized by compact size, wider bandwidth, and higher gain. Additionally, the antenna radiates omnidirectionally and shows good impedance matching (return loss < -10 dB) over the frequency range from 2.1 GHz to 4.35 GHz which covers WLAN (2.4 and 3.6 GHz), WiMax (2.3, 2.5, 3.5 GHz) and most of the bands of 3G and 4G (2.5–2.69 GHz, 3.4–3.69 GHz).

## 2. EXPERIMENTAL

### 2.1. Antenna Design and Analysis

The proposed antenna was designed on a commercially available PET sheet with a dielectric constant 3.2, loss tangent 0.022, and thickness 135  $\mu\text{m}$ . The overall size of the designed antenna is 64 mm  $\times$  42 mm. Figure 1 shows the evolution of the proposed antenna design. The design process started with a conventional CPW fed (50  $\Omega$ ) slotted bowtie structure with symmetric flare angles (Upper flare angle,  $\theta_1$  = Lower flare angle,  $\theta_2 = 25^\circ$ ), as shown in Figure 1(a). The ground and feedline gap parameters

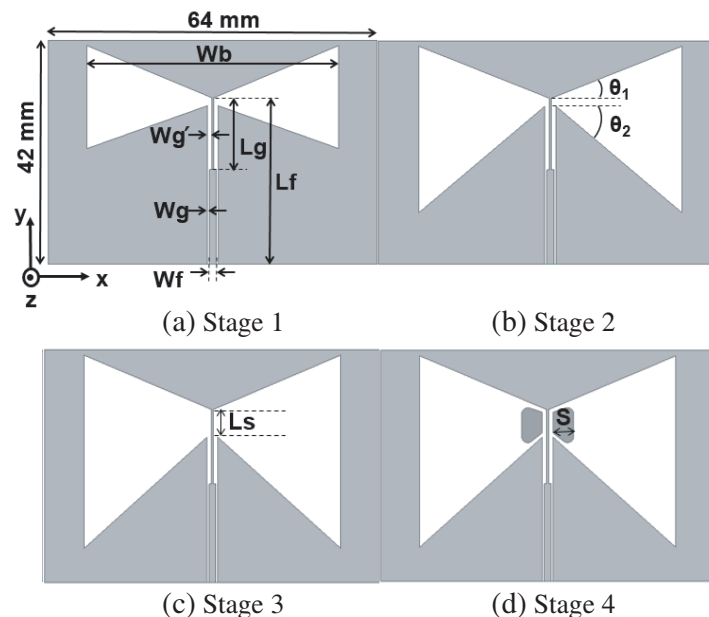
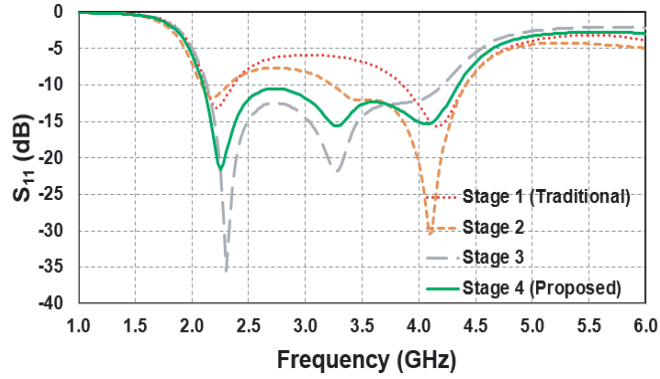


Figure 1. Evolution of the proposed antenna design.

( $Wg, Wg'$ ) and the parameters related to feedline length ( $Lf, Lg$ ) control the position of the resonant frequency. The resonant frequency of the initial structure is at 4.2 GHz. In stage 2 (Figure 1(b)), asymmetric flare angle ( $\theta_1 \neq \theta_2$ ) is introduced in the traditional bowtie structure ( $\theta_1 = 25^\circ, \theta_2 = 40^\circ$ ) to generate a wider bandwidth than the conventional one. A stem width  $Ls$  in stage 3 is poised to improve impedance matching and significantly increase the bandwidth. At the fourth and final stage, two symmetrical metal strips are placed underneath each slot of bowtie to increase the bandwidth further.

The finally achieved  $-10$  dB bandwidth is 2.25 GHz (69.77%) from 2.1 GHz to 4.35 GHz. Figure 2 shows the reflection coefficient ( $S_{11}$ ) plot at different design stages. The ANSYS High-Frequency Structural Simulator (HFSS) simulated final dimensions are given in Table 2.



**Figure 2.** Reflection coefficient plot ( $S_{11}$ ) of the design stages.

**Table 2.** Proposed free space antenna dimension.

Parameters	Dimension	Unit
$Wb$	49	mm
$Wf$	1.3	mm
$Wg$	0.4	mm
$Wg'$	0.85	mm
$Ws$	0.8	mm
$Lf$	31.3	mm
$Lg$	13.5	mm
$\theta_1$	25	Degree
$\theta_2$	40	Degree
$Ls$	5.3	mm
$S$	4	mm

The implementation of the designed antenna is driven by investigating the parameters that impact the frequency response. The parametric study started by varying bowtie slot length  $Wb$  in the initial (traditional) bowtie structure. Figure 3 shows the reflection coefficient versus frequency plot for different values of  $Wb$ . It can be observed that as  $Wb$  increases, the two resonant peaks shift to lower frequencies. Considering impedance matching and target frequency band (2.4 GHz and 3.6 GHz), the bowtie slot length was fixed at  $Wb = 49$  mm. Next, keeping the value of  $Wb$  fixed at 49 mm, the reflection coefficient was inspected by changing the flare angle ( $\theta_2$ ) from  $25^\circ$  to  $45^\circ$ . Figure 4 shows the impact of  $\theta_2$  on the  $S_{11}$  plot. Changing  $\theta_2$  affects the degree of impedance matching significantly. In addition, the increasing  $\theta_2$  broadens the second resonance. The flare angle  $\theta_2 = 40^\circ$  is chosen as the optimum value for this design. In addition to the bowtie slot length and the flare angle, the impact of the feeding neck

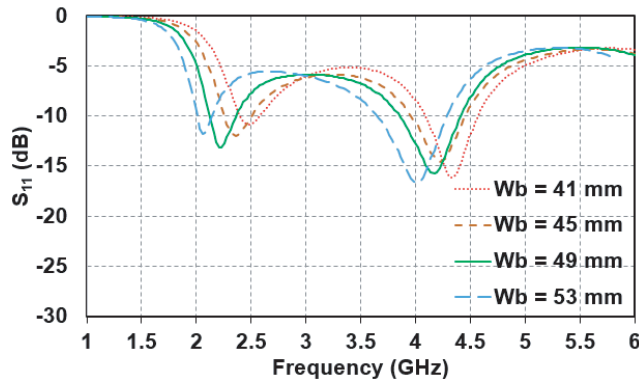


**Figure 3.**  $S_{11}$  response of the initial bowtie structure for different values of  $Wb$ .

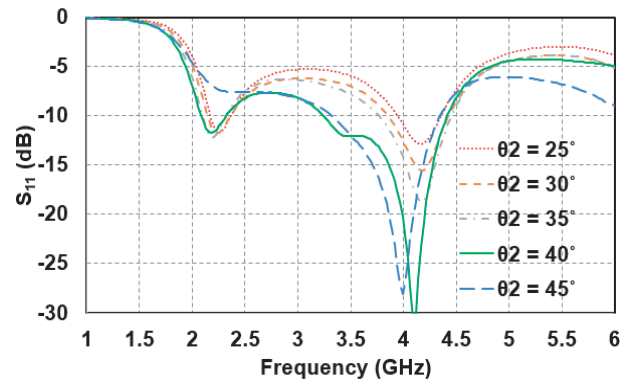


**Figure 4.**  $S_{11}$  response of the design for different values of  $\theta_2$  ( $Wb$  fixed at 49 mm).

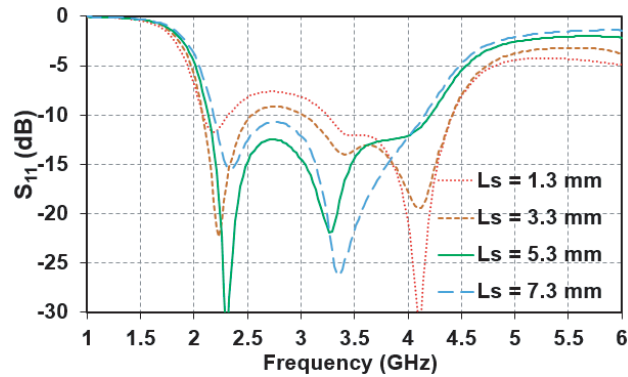


**Figure 5.**  $S_{11}$  response of the design for different values of  $Ls$  ( $Wb$  fixed at 49 mm) respectively).

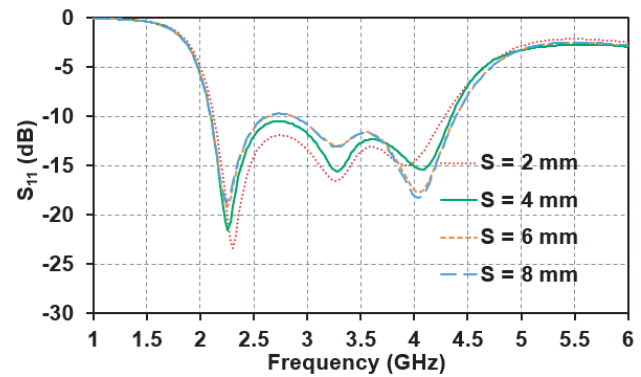


**Figure 6.**  $S_{11}$  response of the design for different values of  $S$  ( $Wb$ ,  $\theta_2$  and  $Ls$  fixed at 49 mm,  $40^\circ$  and 5.3 mm respectively).

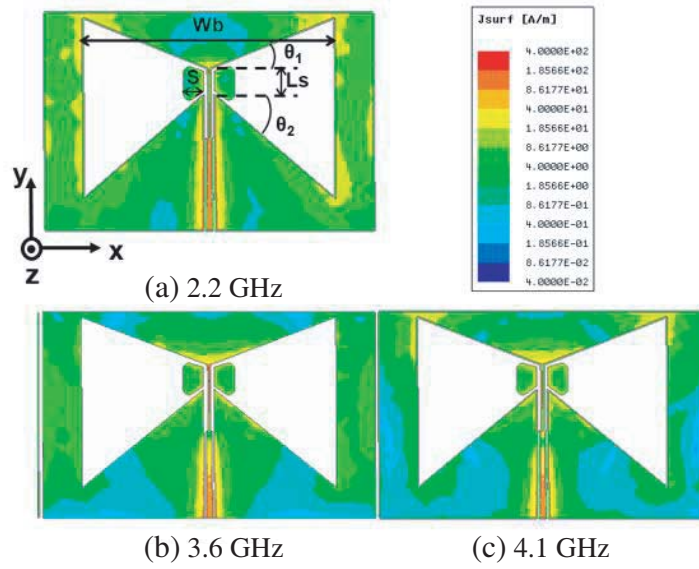
width ( $Ls$ ) on  $S_{11}$  was investigated, keeping  $Wb$  ( $= 49$  mm) and  $\theta_2$  ( $= 40^\circ$ ) constant.

Figure 5 shows an increase in bandwidth as  $Ls$  is increased up to 5.3 mm. Moreover, the second resonant frequency shifts towards the low-frequency region with increasing  $Ls$  value. Finally, the length of the metal strip  $S$  was varied keeping the other parameters at their optimum value. From the  $S_{11}$  plot shown in Figure 6, it can be seen that the bandwidth increases with the increasing value of  $S$ .  $S = 4$  mm generates the highest bandwidth with acceptable impedance performance ( $< -10$  dB) and hence chosen as the optimized value.

From the parametric studies, it is evident that the tuning of bowtie slot length  $Wb$ , lower flare angle  $\theta_2$ , bowtie neck width  $Ls$ , and strip width  $S$  seems to generate a wider bandwidth. Such an observation can be explained from the current distribution plot (Figure 7) of the antenna at three resonant frequency points 2.2 GHz, 3.6 GHz and 4.2 GHz. It can be seen that maximum current density seems to be concentrated at the edge of slots, feeding neck and metal strips of the bowtie structure indicating the tuning of the parameters  $Wb$ ,  $\theta_2$ ,  $Ls$  and  $S$  generated a wider impedance bandwidth. Moreover, it is observed that at lower frequencies, the current distribution is stronger than higher frequencies resulting in better impedance matching in lower operating frequencies.

## 2.2. Fabrication of the Antenna

The designed free space antenna was fabricated using a Fujifilm Dimatix 2831 Inkjet printer (DMP) that offers precise printing using 1 pL and 10 pL volume cartridges. In this experiment, a 10 pL cartridge was used, which has 16 nozzles of diameter 21  $\mu$ m and driven by the piezoelectric element of the Dimatix



**Figure 7.** Current distribution plot of the proposed antenna at different resonant frequencies.

printer. Commercially available silver (Ag) Nanoparticle ink from Novacentrix was used. The ink specifications are Ag content 40 wt%, viscosity 8 to 12 cp and surface tension 19–30 dyne/cm.

Optimized printing parameters were investigated in an earlier study [38], and the results from that study were adopted to print the antenna. The employed optimum printing conditions are given in Table 3. The printed samples were sintered on a hotplate at 120° temperature to generate conductivity and create a compact silver layer. The printed samples were inspected using a Scanning Electron Microscope (SEM) Quanta 3D 200i. Besides, the printed layer thickness was measured using the SEM after cutting a sample using scissors. The fabricated antenna was tested with the Agilent PNA-LN5230C vector network analyzer (VNA) to validate the simulated design.

**Table 3.** Optimal printing parameters.

Parameter	Optimum value
Substrate Temperature	28°C
Cartridge Temperature	28°C
Printer Print Height	750 $\mu\text{m}$
Jetting Frequency	4.4 kHz
Drop Velocity	7–7.5 m/s
Drop Size	10 pL
Drop Spacing/Print Resolution	20 $\mu\text{m}$
No of printing layers	3

### 3. RESULTS AND DISCUSSION

Figure 8 shows the image of the inkjet-printed antenna on the PET substrate. The SEM images (Figures 8(b) and 8(c)) show uniform silver ink distribution on the PET surface with sharp edges ensuring satisfactory printed pattern quality. Figure 8(d) shows the cross-sectional image of the printed antenna. The measured Ag ink layer thickness was found to be 3.69  $\mu\text{m}$ . The reflection coefficient ( $S_{11}$ ) measurement setup and the measured  $S_{11}$  response of the antenna is shown in Figure 9. It is evident that

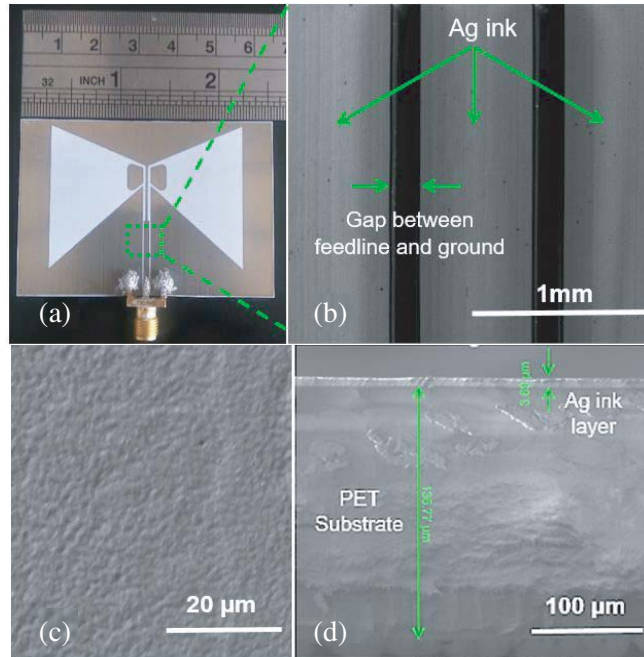


**Figure 8.** Schematic of the ink-jet printed antenna. (a) Photograph of the printed antenna. (b) Magnified SEM image of the printed pattern indicating sharp edges (obtained with 1 mm scale). (c) Surface morphology of the Ag ink surface (obtained with 20  $\mu\text{m}$  scale) and (d) cross section image of the printed pattern (obtained with 20  $\mu\text{m}$  scale).

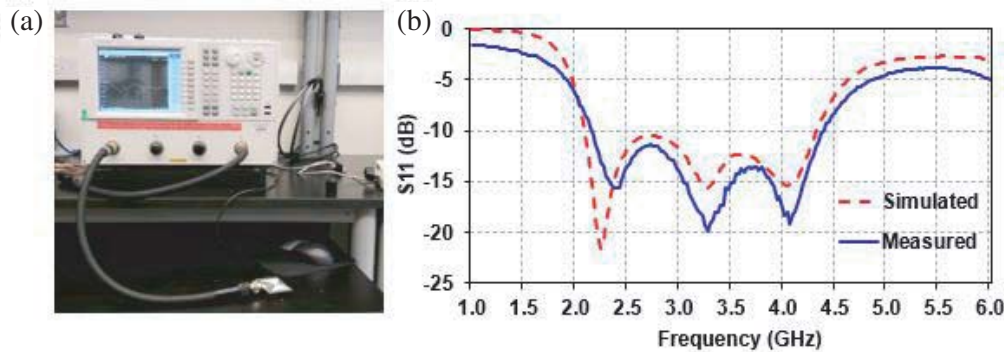


**Figure 9.** Return loss measurement. (a) Return loss measurement system and (b) simulated and measured return loss (dB) of the proposed antenna.

the design has three resonant frequencies: 2.1, 3.3, and 4.1 GHz. The individual operating bandwidths around these frequencies are overlapped, leading to a  $-10$  dB bandwidth from 2.1 to 4.35 GHz (69.77%). The measurement is in good agreement with the simulation with a slight shift in resonant frequencies. The frequency shifts are attributed to the minor imperfections in fabrication. However, the achieved bandwidth covers the target IoT frequency band application.

In addition to the investigation of the return loss, the antenna radiation pattern was also investigated. The proposed antenna simulated radiation pattern (Figure 10) matches with earlier reported work [11, 39], which ensures the validity of the design. Generally, omnidirectional antennas are preferred for most WLAN and IoT applications [40]. From the simulated co-polarized, cross-polarized fields and 3D gain plot, it is observed that the antenna presents omnidirectional characteristics. Besides, the  $x$ - $z$  plane cross-polarization value is 15 to 25 dB lower than the co-polarized values, whereas the cross-

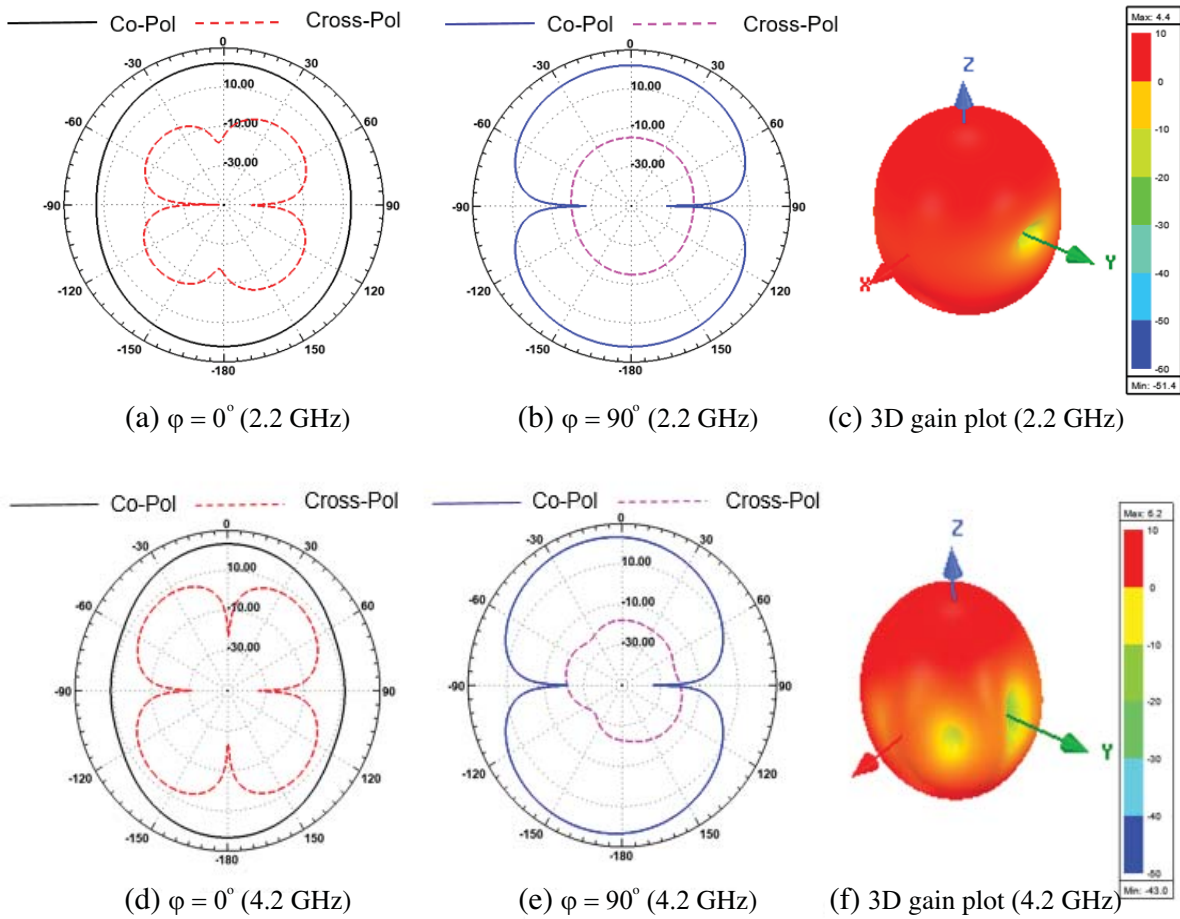


**Figure 10.** Simulated co- and cross-polarization and 3D gain plot. (a)  $x-z$  plane at 2.5 GHz. (b)  $y-z$  plane 2.5 GHz. (c) 3D gain plot at 2.2 GHz. (d)  $x-z$  plane 4.0 GHz. (e)  $y-z$  plane 4.0 GHz. (f) 3D gain plot at 4.2 GHz.

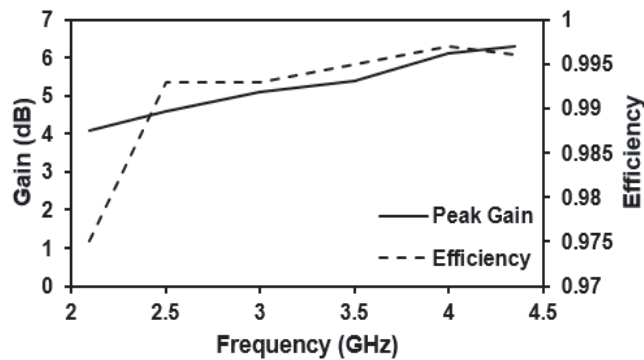


**Figure 11.** Frequency versus gain plot of the proposed antenna.

polarization on the  $y-z$  plane is 25 to 35 dB lower than the co-polarized values for the whole application band. Due to the lack of instrumentation, the authors could not measure the experimental radiation pattern. Figure 11 illustrates the simulated antenna gain and efficiency for the whole application band. Notably, the gain plot shows an increasing trend from lower to higher frequency. At the highest operating frequency (4.35 GHz), the obtained peak gain is 6.3 dB. As expected, the gain is highest at 4.35 GHz

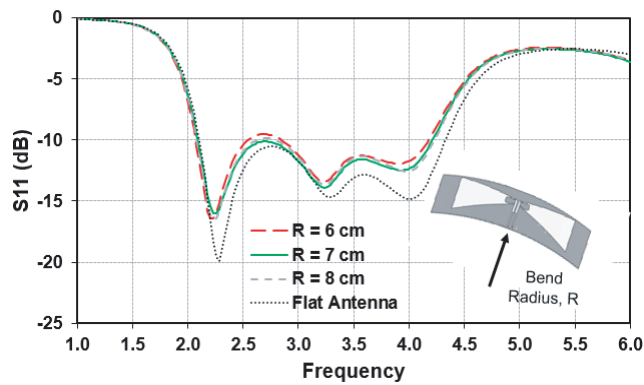


**Figure 12.** Simulated bending impact on antenna return loss at different bending radii.

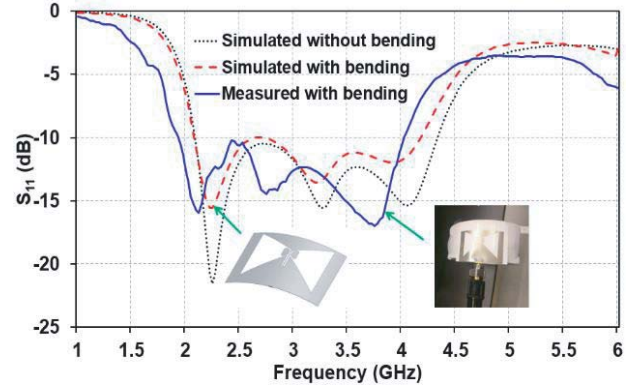


**Figure 13.** Measured bending impact on antenna return loss.

due to the large electrical size of the antenna at that frequency as compared to its size at other lower operating frequencies. On the other hand, the antenna shows high (> 97%) for the whole application band.

The electromagnetic performance of the antenna, mainly the resonant frequency and return loss, needs to be investigated under bent conditions to evaluate the suitability for practical applications. Figure 12 presents the simulated effect of bending at different bending radii  $R$ . Based on the simulation, a shift in resonant frequencies with degraded matching was observed for the bent antenna when compared to the flat configuration. Such an observation is attributed to the fact that bending increases the effective resonant length of the antenna, which in turn, results in shifting the resonance towards lower frequencies. However, it can be adjusted by tuning the antenna parameters. The tuning is demonstrated later in this article.

To investigate the bending practically, the antenna was placed around a cylindrical object of 7 cm radius with permittivity  $\epsilon_r = 1$ . Figure 13 shows the comparison of simulated and measured bending impact on the return loss. During the antenna testing phase, a frequency shift was observed causing degraded impedance matching in higher operating frequencies. This is attributed to the fact that slightly higher permittivity ( $\epsilon_r \approx 1.3$ ) of the used cylindrical structure (on which the antenna was placed) compared to simulation ( $\epsilon_r = 1$ ). As  $\epsilon_r$  increases, the resistive part of input impedance decreases and the reactance becomes capacitive [41]. Yet, the antenna maintains the desired application bandwidth. The antenna exhibits adequate flexibility and mechanical robustness that meet the requirements for practical IoT applications.

Next, the tunability of the designed free space antenna was investigated through simulation for a drywall mounting structure. The given dimension of the drywall is 610 mm  $\times$  610 mm  $\times$  12.7 mm with a dielectric constant  $\epsilon_0 = 2.2$  and loss tangent  $\tan \delta = 0.011$  [42, 43]. Figure 14 shows the simulated  $S_{11}$  response of the free space antenna mounted on drywall. Because of the higher dielectric constant of the drywall ( $\approx 2.2$ ) than the free space ( $= 1$ ), it is observed that the bandwidth of the antenna shifts to the lower frequency region causing high insertion loss at higher operating frequencies ( $> 3.6$  GHz). To shift the reflection coefficient to the desired frequency band, the antenna parameters bowtie slot length  $Wb$ , the gap between feedline and ground  $Wg$ , flare angles  $\theta_1$ , and  $\theta_2$  are tuned. After tuning, the value of  $Wb$  is reduced to 32.3 mm from 49 mm and for  $Wg'$ , the value is increased to 0.95 mm from 0.85 mm. Along with these, upper ( $\theta_1$ ) and lower ( $\theta_2$ ) flare angle values are increased to 31.5° and 47.6° from the initially designed values. After adjusting the parameters, it can be seen that both versions (free space and tuned drywall mounted) cover the entire targeted bandwidth (Figure 14).

In addition, the overall size of the antenna is reduced from 64 mm  $\times$  42 mm to 42.9 mm  $\times$  42 mm when mounted on drywall. The parent antenna could be easily re-tuned for other support structures like wood, brick, etc. Table 4 shows a comparison of the free space antenna performance with the previously reported flexible bowtie antennas in a similar frequency band. It shows that the proposed antenna has a wider bandwidth compared to other flexible bowtie antennas. Moreover, the peak gain is also higher than most of the reported antennas.

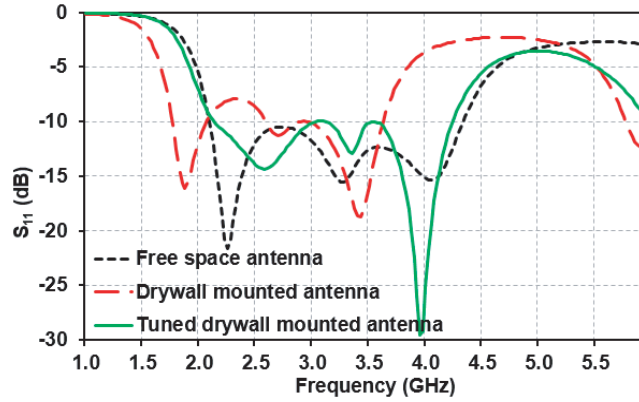


**Figure 14.**  $S_{11}$  response for the proposed antenna on drywall.

**Table 4.** Comparison with the flexible bow-tie antennas presented in the literature in similar frequency range.

References	Substrate permittivity, $\epsilon_r$	Size (mm)	Operating range (GHz)	FBW %	Peak gain (dB)
Sallam et al. [21]	3.38	$80 \times 60$	2.2–4.0	57.7	6.2
Liu et al. [22]	2.2	$55 \times 25$	3.4–3.6	6.0	N/A
Farooqui et al. [25]	1.9	$88 \times 44$	2.54–3.0	16.6	0.8
Chowdhary et al. [26]	3.38	$80 \times 60$	3.0–4.87	59.5	7.82
<b>This work</b>	<b>3.2</b>	<b><math>64 \times 42</math></b>	<b>2.1–4.35</b>	<b>69.77</b>	<b>6.3</b>

#### 4. CONCLUSIONS

In this study, a new wideband bowtie slot antenna on a flexible PET substrate was designed and implemented. The antenna was designed for free space and drywall mounted application at WLAN, WiMax, 3G, and 4G frequency bands. The designed antenna exhibits an improved performance compared to the other flexible bowtie antennas available in the literature. For both designs, the antenna exhibits a wider bandwidth ( $> 65\%$ ). The free space antenna was fabricated and validated through simulation and measurement results. The antenna radiates omnidirectionally with a peak gain of 6.3 dB at 4.35 GHz. The bending test of the antenna indicates mechanical robustness, making it a candidate for IoT applications.

#### REFERENCES

- Hester, J. G. and M. M. Tentzeris, “Inkjet-printed flexible mm-wave Van-Atta reflectarrays: A solution for ultralong-range dense multitag and multisensing chipless RFID implementations for IoT smart skins,” *IEEE Transactions on Microwave Theory and Techniques*, Vol. 64, No. 12, 4763–4773, 2016.
- Paracha, K. N., S. K. A. Rahim, H. T. Chattha, S. S. Aljaafreh, and Y. C. Lo, “Low-cost printed flexible antenna by using an office printer for conformal applications,” *International Journal of Antennas and Propagation*, Vol. 2018, 1–7, 2018.
- Li, X., M. M. Honari, Y. Fu, A. Kumar, H. Saghlatoon, P. Mousavi, and H.-J. Chung, “Self-reinforcing graphene coatings on 3D printed elastomers for flexible radio frequency antennas and strain sensors,” *Flexible and Printed Electronics*, Vol. 2, No. 3, 035001, 2017.

4. Cosker, M., L. Lizzi, F. Ferrero, R., Staraj, and J.-M. Ribero, "Realization of 3-D flexible antennas using liquid metal and additive printing technologies," *IEEE Antennas and Wireless Propagation Letters*, Vol. 16, 971–974, 2016.
5. Abutarboush, H. F. and A. Shamim, "Based inkjet-printed tri-band U-slot monopole antenna for wireless applications," *IEEE Antennas and Wireless Propagation Letters*, Vol. 11, 1234–1237, 2012.
6. Mansour, A., N. Shehata, B. Hamza, and M. Rizk, "Efficient design of flexible and low cost paper-based inkjet-printed antenna," *International Journal of Antennas and Propagation*, Vol. 2015, 2015.
7. Anagnostou, D. E., A. A. Gheethan, A. K. Amert, and K. W. Whites, "A direct-write printed antenna on paper-based organic substrate for flexible displays and WLAN applications," *Journal of Display Technology*, Vol. 6, No. 11, 558–564, 2010.
8. Hassan, A., S. Ali, G. Hassan, J. Bae, and C. H. Lee, "Inkjet-printed antenna on thin PET substrate for dual band Wi-Fi communications," *Microsystem Technologies*, Vol. 23, No. 8, 3701–3709, 2017.
9. Guo, X., Y. Hang, Z. Xie, C. Wu, L. Gao, and C. Liu, "Flexible and wearable 2.45 GHz CPW-fed antenna using inkjet-printing of silver nanoparticles on pet substrate," *Microwave and Optical Technology Letters*, Vol. 59, No. 1, 204–208, 2017.
10. Huang, C.-Y. and D.-Y. Lin, "CPW-fed bowtie slot antenna for ultra-wideband communications," *Electronics Letters*, Vol. 42, No. 19, 1073–1074, 2006.
11. Bhaskar, V. S., E. L. Tan, and L. K. H. Holden, "Design of wideband bowtie slot antenna using sectorially modified gielis curves," *IEEE Antennas and Wireless Propagation Letters*, Vol. 17, No. 12, 2237–2240, 2018.
12. Mazaheri, M., N. Amani, and A. Jafargholi, "Wideband printed slot bowtie antenna using symmetric vias," *Microwave and Optical Technology Letters*, Vol. 58, No. 6, 1301–1304, 2016.
13. Pierce, R. G., A. J. Blanchard, and R. M. Henderson, "Broadband planar modified aperture bowtie antenna," *IEEE Antennas and Wireless Propagation Letters*, Vol. 12, 1432–1435, 2013.
14. Tsai, L.-C., "A triple-band bow-tie-shaped CPW-fed slot antenna for WLAN applications," *Progress In Electromagnetics Research C*, Vol. 47, 167–171, 2014.
15. Xu, L., L. Li, and W. Zhang, "Study and design of broadband bowtie slot antenna fed with asymmetric CPW," *IEEE Transactions on Antennas and Propagation*, Vol. 63, No. 2, 760–765, 2014.
16. Chen, Y.-L., C.-L. Ruan, and L. Peng, "A novel ultra-wideband bow-tie slot antenna in wireless communication systems," *Progress In Electromagnetics Research Letters*, Vol. 1, 101–108, 2008.
17. Yoon, J. H., and Y. C. Lee, "Modified bowtie slot antenna for the 2.4/5.2/5.8 GHz WLAN bands with a rectangular tuning stub," *Microwave and Optical Technology Letters*, Vol. 53, No. 1, 126–130, 2011.
18. Dayo, Z. A., Q. Cao, P. Soothar, M. M. Lodro, and Y. Li, *A Compact Coplanar Waveguide Feed Bowtie Slot Antenna for WIMAX, C and X Band Applications*, 1–3, IEEE, 2019.
19. Yamamoto, M. and T. Nojima, *Design of a Leaf-shaped Bowtie Slot Antenna Electromagnetically Fed by a Microstrip Line*, 261–262, IEEE, 2014.
20. Sagnard, F. and F. Rejiba, "Wide band coplanar waveguide-fed bowtie slot antenna for a large range of ground penetrating radar applications," *IET Microwaves, Antennas and Propagation*, Vol. 5, No. 6, 734–739, 2011.
21. Sallam, M. O., S. M. Kandil, V. Volski, G. A. Vandenbosch, and E. A. Soliman, "Wideband CPW-fed flexible bowtie slot antenna for WLAN/WiMax systems," *IEEE Transactions on Antennas and Propagation*, Vol. 65, No. 8, 4274–4277, 2017.
22. Liu, H., S. Zhu, P. Wen, X. Xiao, W. Che, and X. Guan, "Flexible CPW-fed fishtail-shaped antenna for dual-band applications," *IEEE Antennas and Wireless Propagation Letters*, Vol. 13, 770–773, 2014.
23. Sahoo, R. and D. Vakula, "Bow-tie-shaped wideband conformal antenna with wide-slot for GPS application," *Turkish Journal of Electrical Engineering & Computer Sciences*, Vol. 27, No. 1, 80–93, 2019.

24. Durgun, A. C., M. S. Reese, C. A. Balanis, C. R. Birtcher, D. R. Allee, and S. Venugopal, *Book Flexible Bowtie Antennas with Reduced Metallization*, 50–53, IEEE, 2011.
25. Farooqui, M. F. and A. Shamim, *Dual Band Inkjet Printed Bowtie Slot Antenna on Leather*, 3287–3290, IEEE, 2013.
26. Choudhary, E., S. Sharma, and P. Yadav, *A Modified Wideband Bow-tie Antenna with DGS for Wireless Fidelity Range*, 1–5, IEEE, 2018.
27. Salonen, P., J. Kim, and Y. Rahmat-Samii, *Dual-band E-shaped Patch Wearable Textile Antenna*, 466–469, IEEE, 2005.
28. Singh, N., A. K. Singh, and V. K. Singh, “Design and performance of wearable ultrawide band textile antenna for medical applications,” *Microwave and Optical Technology Letters*, Vol. 57, No. 7, 1553–1557, 2015.
29. Krykpayev, B., M. F. Farooqui, R. M. Bilal, M. Vaseem, and A. Shamim, “A wearable tracking device inkjet-printed on textile,” *Microelectronics Journal*, Vol. 65, 40–48, 2017.
30. Mansour, A., M. Azab, and N. Shehata, *Flexible Paper-based Wideband Antenna for Compact-size IoT Devices*, 426–429, IEEE, 2017.
31. Zahran, S. R., Z. Hu, and M. A. Abdalla, *A Flexible Circular Polarized Wide Band Slot Antenna for Indoor IoT Applications*, 1163–1164, IEEE, 2017.
32. Lee, C.-H., S.-Y. Chen, and P. Hsu, *Compact Modified Bowtie Slot Antenna Fed by CPW for Ultra-wideband Applications*, 1–4, IEEE, 2009.
33. Qu, S.-W. and C.-L. Ruan, “Effect of round corners on bowtie antennas,” *Progress In Electromagnetics Research*, Vol. 57, 179–195, 2006.
34. Saha, T. K., T. N. Knaus, A. Khosla, and P. K. Sekhar, “A CPW-fed flexible UWB antenna for IoT applications,” *Microsystem Technologies*, 1–7, 2018.
35. Elobaid, H. A. E., S. K. A. Rahim, M. Himdi, X. Castel, and M. A. Kasgari, “A transparent and flexible polymer-fabric tissue UWB antenna for future wireless networks,” *IEEE Antennas and Wireless Propagation Letters*, Vol. 16, 1333–1336, 2016.
36. Jilani, S. F. and A. Alomainy, *Planar Millimeter-wave Antenna on Low-cost Flexible PET Substrate for 5G Applications*, 1–3, IEEE, 2016.
37. Lee, C. M., Y. Kim, Y. Kim, I. K. Kim, and C. W. Jung, “A flexible and transparent antenna on a polyamide substrate for laptop computers,” *Microwave and Optical Technology Letters*, Vol. 57, No. 5, 1038–1042, 2015.
38. Riheen, M. A., T. K. Saha, and P. K. Sekhar, “Inkjet printing on PET substrate,” *Journal of the Electrochemical Society*, Vol. 166, No. 9, B3036–B3039, 2019.
39. Saha, T. K., C. Goodbody, T. Karacolak, and P. K. Sekhar, “A compact monopole antenna for ultra-wideband applications,” *Microwave and Optical Technology Letters*, Vol. 61, No. 1, 182–186, 2019.
40. De Cos Gómez, M., H. F. Álvarez, C. G. González, B. P. Valcarce, J. Olenick, and F. Las-Heras, *Ultra-thin Compact Flexible Antenna for IoT Applications*, 1–4, IEEE, 2019.
41. Katehi, P. and N. Alexopoulos, “On the effect of substrate thickness and permittivity on printed circuit dipole properties,” *IEEE Transactions on Antennas and Propagation*, Vol. 31, No. 1, 34–39, 1983.
42. Thajudeen, C., A. Hoorfar, F. Ahmad, and T. Dogaru, “Measured complex permittivity of walls with different hydration levels and the effect on power estimation of TWRI target returns,” *Progress In Electromagnetics Research B*, Vol. 30, 177–199, 2011.
43. Common, L. T., “Propagation losses through common building materials 2.4 GHz vs 5 GHz,” E10589, Magis Network, Inc., 2002.